

Quasiparticle Density of States Measurements in Clean Superconducting AlMn Alloys*

G. C. O’Neil,[†] D. R. Schmidt, N. A. Tomlin, and J. N. Ullom

NIST, Boulder

(Dated: July 27, 2009)

Aluminum doped with Manganese (AlMn) forms a superconducting alloy with the transition temperature suppressed by the added Manganese. We present quasiparticle density of states measurements on superconducting AlMn alloys made by current-voltage measurements on normal-metal/insulator/superconductor tunnel junctions. The density of states remains BCS-like with a reduced gap, matching the predictions of Kaiser. However we measure additional subgap states not predicted by Kaiser, and demonstrate that these subgap states will harm some potential applications.

I. INTRODUCTION

Impurities in solids are widely studied in part because they offer the opportunity to alter and sometimes improve material properties. The description of impurities in s-wave superconductors begins with the Anderson model where ions with a localized magnetic moment from d-band states are dissolved in a nonmagnetic host¹. Whether the impurities retain their magnetic character in the host depends largely on the relative magnitude of the width, Λ , of the localized electronic states after hybridization with the conduction electrons and the splitting, ν , of the localized spin-up and -down states due to Coulomb repulsion. For $\Lambda \ll \nu$, the well known result of Abrikosov and Gor’kov² (AG) is obtained in which impurities retain their magnetic character and suppress the critical temperature T_c and energy gap Δ . A defining characteristic of this regime is that the quasiparticle density of states (DOS) is heavily distorted and, in particular, the singularity at the gap-edge is smoothed out for any appreciable suppression of T_c . For $\Lambda \gg \nu$, localized spin-up and -down states are equally populated and the impurities lose their magnetic character. This regime is considerably less well studied, but has been described by Kaiser³. In recent work, by O’Neil et al., an important prediction of the theory of Kaiser was verified; namely that nonmagnetic impurities can significantly suppress T_c and Δ while retaining a BCS-like DOS⁴. This prediction was verified by measurements of electronic tunneling into superconducting Al films doped with Mn.

The measurements of O’Neil et al. showed increased sub-gap states and gap-edge smearing compared to Kaiser’s DOS predictions. It was suspected that some portion of the deviation from Kaiser’s DOS predictions was due to additional non-Mn impurities in the Al. Here we present additional tunneling measurements on cleaner AlMn films. Our results show that the unwanted impurities were causing significant distortion to the DOS. However, measurements from cleaner AlMn still show sub-gap

states and gap-edge smearing at a significant level.

The ability to vary the properties of superconductors is often useful. For example, the ability to tune T_c of a proximity-coupled superconductor-normal metal bilayer has enabled resistive thermometers for experiments ranging from the search for weakly interacting dark matter⁵ to alpha particle detectors for nuclear forensics⁶. Some types of low temperature devices exploit the highly non-linear DOS found in a BCS superconductor, and for these devices, the use of nonmagnetic impurities to tune Δ while preserving the gap-edge singularity in the DOS is attractive. Thin-film electron-tunneling refrigerators are one such type of device^{7,8}.

Electron tunneling refrigerators use the singularity at the gap-edge of the density of states as a filter to selectively remove the hottest electrons from a normal metal. To date, Al has been used as the superconductor in these devices because of its desirable oxide properties and because Δ in Al is optimally sized for cooling from 300 mK. Thermal modeling shows that cooling from 100 mK would work better with a superconductor with a smaller Δ than Al. While Al is well suited for cooling from 300 mK, the ability to controllably suppress Δ while retaining a BCS-like DOS raises the possibility of improved cooling below 100 mK without losing the oxide properties of Al. We present DOS measurements via normal-metal/insulator/superconductor tunneling which show that AlMn will not cool better than Al below 100 mK because Mn doping introduces additional sub-gap states.

II. METHODS

We make superconductor/insulator/normal-metal/insulator/superconductor (SINIS) tunnel junctions where the superconducting electrodes are either elemental Al or AlMn. The low temperature current-voltage relation of SINIS junctions depends strongly on the DOS of the superconducting electrode. We chose not to use the superconductor/insulator/superconductor (SIS) tunneling technique because of (1) snapping to the supercurrent branch of the current-voltage curve when probing the deep sub-gap, (2) backbending in the

*Contribution of a U.S. government agency, not subject to copyright.

	Mn	Fe	Co	Cu	In	W	Si
T1	3000	81	196	37	< 0.1	0.7	67
T2	3900	9	4	510	194	29	37
T3	4200	10	1	19	1.7	2.9	30
Al	.03	.14	< .005	.13	< .002	< .002	.7

TABLE I: This table shows some of the impurities measured in each of the AlMn sputter deposition targets in parts per million by number of atom. These concentrations were measured with Glow Discharge Mass Spectroscopy (GDMS), and carry an uncertainty of $\pm 20\%$. The Mn concentrations were measured with Inductively Coupled Plasma Mass Spectroscopy with an uncertainty of $\pm 3\%$. The impurity concentrations in the Al target are from GDMS measurements provided by the manufacturer. All impurities not shown are below 10 ppm.

current-voltage relation at the gap edge due to high injected quasiparticle densities that prevents interpretation of the data⁹, and (3) the higher sub-gap resistances of SIS junctions that require amplifiers with greater input impedance.

Co-sputtering is used to study DOS as a function of Mn concentration in Al. We co-sputter from an elemental Al target and an AlMn target with ~ 4200 ppm (by number of atoms) of Mn. By varying the sputter rates from each target independently, we can achieve any concentration from zero to the full concentration of the AlMn target. We calculate the concentration of the deposited AlMn based on previous measurements of the deposition rates of the two sputter guns. Three different AlMn sputter targets were used for these measurements, referred to as T1, T2, and T3. The AlMn targets were purchased commercially and prepared by vacuum melting. We sent a sample of the source material from each target another commercial lab for analysis. The results of these analyses are shown in Table I along with results from an elemental Al sputter target. Targets T1 and T2 had significant unwanted impurities, while target T3 is has no impurities above the 30 ppm level. Target T1 was used in earlier work that led to the effort described in this paper to use cleaner AlMn⁴. Target T3 is the cleanest target we were able to purchase.

The SINIS structures are fabricated on 75 mm oxidized silicon wafers. A 50 nm film of AlMn is deposited on the wafer to form the normal-metal base electrode. We use standard photo-lithography techniques to pattern the base electrode and all subsequent layers. The base electrode is wet etched. Then we deposit SiO₂ to form an insulating layer, and use a plasma etch to create vias, which define the junction locations, over the base electrode. The wafer is then placed in a deposition system where it is ion milled to remove the native oxide that has formed on the base electrode. The wafer is moved to the load lock where it is exposed to high purity O₂ gas to grow the tunnel barrier oxide. A typical wafer sees 0.7 kPa (5 Torr) for 20 minutes. Then

the wafer is returned to the deposition chamber, without breaking vacuum, and the superconducting electrode is deposited. The superconducting electrode is 500 nm of Al or co-sputtered AlMn. A typical SINIS structure for these measurements contains two $7 \times 7 \mu\text{m}^2$ junctions in series, with a total normal state resistance of 100 Ω . We try to achieve high resistance-area products to minimize the effects of self cooling on the current-voltage relations.

Completed devices are cooled in an adiabatic demagnetization refrigerator (ADR) with a base temperature of about 60 mK. Four wire measurements of the current-voltage relations of the SINIS tunnel junctions are recorded at many temperatures between the base temperature and T_c . A programmable voltage source and a 0.1-10 M Ω bias resistor are used to provide a current bias. The SINIS current is determined by measuring the voltage across the bias resistor. The SINIS voltage is measured with a nanovoltmeter. The T_c of the counter electrodes of each SINIS device are determined from resistance measurements vs temperature.

The DOS is extracted from the current-voltage relations by comparison to theory. We parameterize the normalized DOS, N_S , for energy E by,

$$N_S(E) = \text{Re} \frac{(E - i\Gamma)}{\sqrt{(E - i\Gamma)^2 - \Delta^2}}. \quad (1)$$

This is the familiar BCS relation with a small imaginary component, Γ , added to the energy. The Dynes parameter, Γ , represents smearing of the BCS gap edge singularity and additional states in the sub-gap region due to finite quasiparticle lifetime¹⁰. If the smearing is caused solely by finite quasiparticle lifetimes, then the uncertainty relationship gives $\tau_R \Gamma = \hbar$, where τ_R is the quasiparticle relaxation time.

The current voltage relationship for a single NIS junction whose normal electrode is at temperature T is

$$I(V, T) = \frac{1}{eR_N} \int_{-\infty}^{\infty} N_S(E - eV) [f(E - eV, T) - f(E, T)] dE, \quad (2)$$

where V is the voltage across the junction, R_N is the resistance of the junction at temperatures above T_c , e is the electron charge, $N_S(E)$ is the normalized DOS in the superconducting electrode, E is the excitation energy relative to the fermi level, and $f(E, T)$ is the fermi function¹¹. The current-voltage relationship is diode-like with very low current in the sub-gap region where $V < \Delta/e$. The current rises sharply near $V = \Delta/e$, and for $V \gg \Delta/e$ the junction behaves like a resistor with resistance R_N . Because the current is symmetric in voltage, it is easy to extend analysis to SINIS structures. Self cooling causes T to be colder than the temperature of the ADR. We correct for this by solving for T with a model for power balance in NIS refrigerators¹². The devices shown here self cool from a bath temperature of 75 mK to 45-55 mK at the optimal cooling bias. The optimal cooling bias occurs near $V = 0.9 \cdot \Delta/e$. The self cooling depends on many parameters of the SINIS junctions including R_N ,

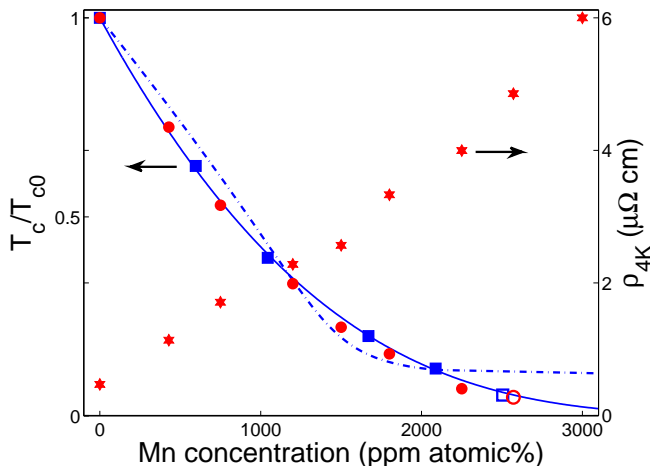


FIG. 1: T_c measured vs Mn concentration in samples made with target T1 (red circles) and target T3 (blue squares). Open markers indicate upper limits for T_c at those concentrations. The solid line is Kaiser's model with parameters $\lambda = 0.187$ and $x_c = 7246$ ppm. The dashed line is AG theory with parameters $x_c = 1368$ ppm and $\delta = .0272$. The parameters for both Kaiser and AG are defined in our previous work⁴, and were determined by least squares fits to the data from target T3 (blue squares). The T_c data follows the Kaiser theory much better than the AG theory. Solid red stars show low temperature resistivity vs concentration for samples from the T1 target. Resistivity at a given concentration should be similar for each target because the total non-Mn impurities are a small fraction of the Mn impurities.

Γ , Δ , and the quasiparticle return parameter β defined by Clark¹². The effect of self cooling on the sub-gap behavior is small at 75 mK.

III. T_c AND RESISTIVITY RESULTS

Prior to junction fabrication, the dependence of T_c on Mn concentration was assessed using a set of 10 μm wide and 100 μm long AlMn resistors with different concentrations of Mn. For each resistor we measured T_c , room temperature resistance and 4 K resistance. Resistivity, ρ , is calculated by RA/L where A is the cross sectional area and L is the length of a resistor.

Figure 1 shows T_c and 4 K resistivity vs Mn concentration, along with predictions by both AG and Kaiser theory. The definitions of the fitting parameters are found in previous work⁴. These data do not concern the primary focus of this paper, which is sub-gap states. We present these data because they may be useful, and because they are more accurate than the similar data presented in our previous work.

IV. CURRENT-VOLTAGE RESULTS

We use current-voltage data taken at 75 mK and the model described in section II to determine Δ and Γ . At

75 mK Δ is equal to its zero temperature value Δ_0 for all samples measured. Low temperatures are desirable because the current-voltage curves are more affected by thermal smearing and self cooling at higher temperatures and the role of Γ is obscured. Normal state resistance, R_N , depends on the oxide thickness and junction area, and is easily measured either above T_c or at voltages greater than $2\Delta/e$. The energy gap, Δ , primarily affects the voltage at which the current sharply increases. The Dynes parameter, Γ , primarily affects the level of current in the sub-gap region and also smears the features at the gap. Figure 2 shows measured current-voltage relations for 3 SINIS devices along with the best fit theory curves used to extract Δ and Γ . The ratio $\Delta/(k_b T_c) = 1.9$ was found to be constant with Mn doping.

Figure 3 shows extracted values of Γ vs T_c from the best examples of SINIS devices made with many source targets and with values of Δ from 60 μeV to 190 μeV . An inset shows a larger number of devices, including devices with poor oxide characteristics. Pinholes and other defects in the oxide tunnel barriers can cause an increase in sub-gap conductance that looks like an increased Γ . No known mechanism can cause a decrease in sub-gap conductance below that given by the DOS. Therefore we feel justified in picking out the lowest Γ value for each class of device (Δ and source target) as the best measurement of the fundamental value of Γ . The value of Γ for elemental Al is about an order of magnitude below that of the value for any doped AlMn sample. In addition samples made from target T1 had significantly higher Γ than those from T2 and T3. Differences between results from targets T2 and T3 fall within experimental uncertainty. Finally, devices with Δ reduced to 80 μeV show slightly higher Γ values than 120 μeV devices.

V. DISCUSSION

These data show that most of the gap suppression in AlMn is not magnetic in origin, consistent with our earlier work. The DOS is much too sharp for the AG mechanism, and the suppression of T_c with Mn concentration is inconsistent with AG. However, our results are not a full confirmation of Kaiser's theory. The observed values of Γ produce gap-edge smearing larger than that predicted by Kaiser. Figure 4 shows a comparison of Kaiser's theory to Equation 1 for material with Δ reduced to 86 μeV . Kaiser predicts less smearing at the gap edge and does not predict any sub-gap states.

Whether the elevated Γ values that we observe are caused by the Mn doping, or by effects not included in Kaiser's theory such as the trace impurities other than Mn, or simple disorder is unclear. In regards to the possible role of impurities other than Mn, targets T2 and T3 have similar Γ values, but target T3 has lower concentrations of Co, Cu, In and W, suggesting that these elements do not strongly contribute to Γ . Our measurements do show that impurities of Fe and Co produce

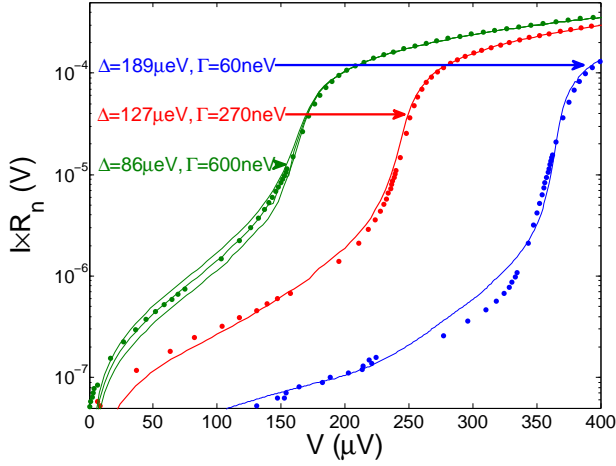


FIG. 2: Measured current-voltage relations (dots) plotted with self-cooling SINIS theory (solid lines). The primary parameters that go into these curves are Δ which affects the voltage at which the current rises, and Γ which affects the level of the current in the sub-gap. The devices with Δ equal to 86 μeV and 127 μeV were made with target T3, while the device with Δ equal to 189 μeV was made with elemental Al. Two additional theory curves are included for the left most ($\Delta=86 \mu\text{eV}$) data set. These curves are generated with values of Γ equal to 1.2 and 0.8 times the best fit value. These additional curves are shown to provide an estimate of uncertainty for Γ , which we place at about $\pm 20\%$.

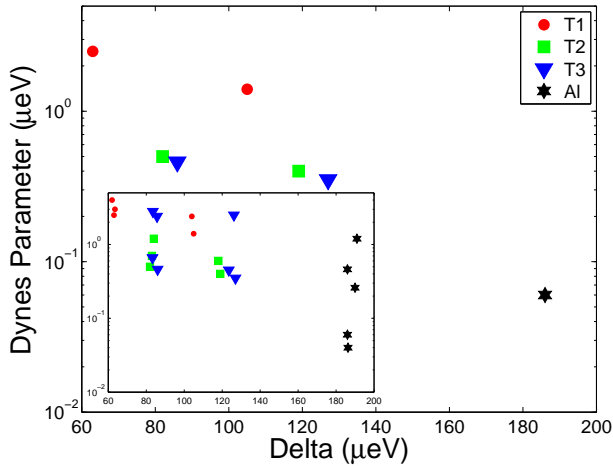


FIG. 3: Measured Γ vs measured Δ for many SINIS structures. Markers correspond to the target used to deposit the superconducting electrode as shown in legend. The inset shows the same data for all SINIS structures measured for this study as well as some historical elemental Al devices.

elevated Γ values because of the nature of these elements rather than because of the disorder introduced by their presence. Target T1 contains fewer impurities than target T2 by atomic ppm, but produces measurably higher Γ values, presumably due to the higher concentrations of Fe and Co in T1.

In regards to the possible role of disorder, the measurements of Barends et al. show that disorder in an Al film can shorten quasiparticle lifetimes¹³. If Dyne's original

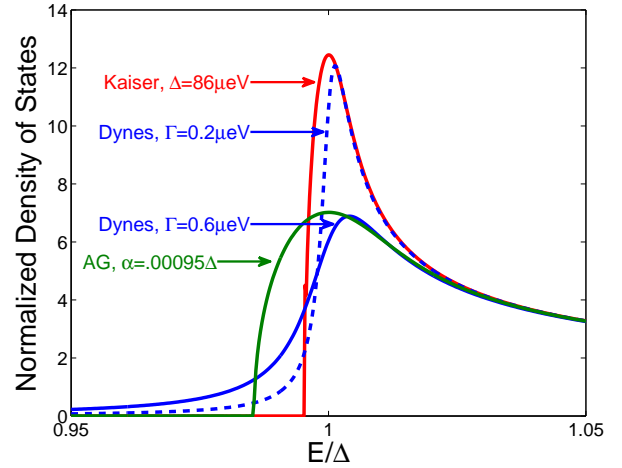


FIG. 4: Comparison of various theories' predictions of density of states. The Kaiser theory was generated using parameters similar to those in Kaiser's original paper, altered to reduce Δ to 86 μeV . The two Dynes curves are generated from Equation 1 using $\Delta=86 \mu\text{eV}$ and the shown values of Γ . One Dynes curve has Γ of 0.6 μeV , which is the measured value for Δ of 86 μeV . The second Dynes curve has Γ 0.6 μeV , determined by a least squares fit to the shown Kaiser curve. AG theory is shown with a value of α , the pair breaking parameter, determined by a least squares fit to the Dynes curve with Γ of 0.6 μeV .

linkage between shortened quasiparticle lifetime and elevated Γ is maintained, then the disorder introduced by Mn doping may be responsible for the elevated Γ values that we observe. The number of defects in the Al films studied by Barends is much smaller than in this work, preventing direct comparison.

It is also possible (or not) that Mn impurities retain a weak magnetic character. In this view, AlMn alloys can be viewed as BCS superconductors with a reduced gap due to the dominant nonmagnetic scattering and elevated α values from low levels of magnetic scattering, where 2α is the effective pair breaking energy in AG theory². Figure 4 compares AG to the measured DOS in a $\Delta=86 \mu\text{eV}$ device, AG can explain the gap-edge smearing but does not predict sub-gap states. The value of α that would explain the gap-edge smearing does not affect T_c . Other theoretical models besides those of Kaiser and AG may be relevant. Both Shiba¹⁴ and ZBMH¹⁵ predict sub-gap states forming as impurity bands in the sub-gap DOS. We have not attempted quantitative comparison to these models because our measurements are well fit by a simple continuum of sub-gap states. Kozorezov¹⁶ has predicted that sub-gap states localized on magnetic impurities can significantly reduce quasiparticle lifetimes, which may increase Γ .

As far as we know, all tunnel junction based measurements of the value of Γ of elemental Al exceed 10 neV. By the uncertainty relationship, this value correspond to a quasiparticle lifetime of 65 ns, which is about 30,000 times less than that measured by Barends et al., with a method not involving tunnel junctions¹³. Therefore all

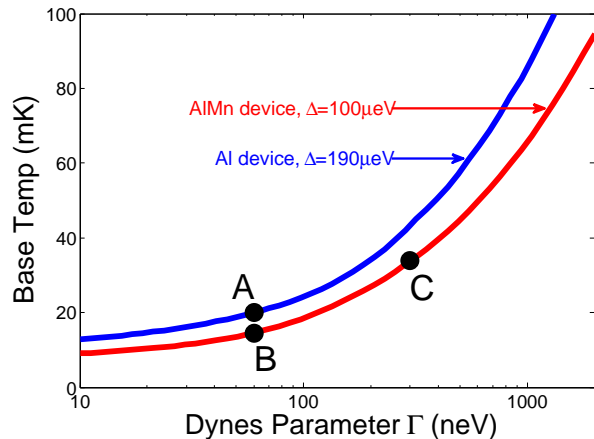


FIG. 5: Theoretical base temperature of an NIS refrigerator when cooling from a bath of 100 mK vs Γ for two different superconducting electrodes, Al with Δ (T_c)=190 μ eV (1.2 K) and AlMn with Δ (T_c)=100 μ eV (0.6 K). The quasiparticle return parameter defined by Clark¹², β , is set to 0.001 in these calculations. The point labeled A indicates that an Al based NIS refrigerator should be able to cool to about 20 mK. Point B indicates that an AlMn based refrigerator could cool to 15 mK if T_c and Δ were reduced without increasing Γ . Point C indicates that the AlMn based refrigerator will cool to only 30 mK with a value of Γ (300 neV) extrapolated from our measurements.

junction-obtained values of Γ in elemental Al are probably dominated by effects related to barrier defects. A critic might claim that all of our results are simply measurements of barrier defects. Our barriers are achieved by oxidizing the base electrode, which is always AlMn with the Mn concentration chosen to drive the electrode fully normal. The fraction of Mn in the junction oxide is independent of the Δ of the superconducting electrode. We can discount the possibility that the increased Γ values that we observe with increased doping values are simply caused by larger numbers of barrier defects.

VI. NIS REFRIGERATOR PERFORMANCE IMPLICATIONS

Electron tunneling NIS junction refrigerators are an attractive technology for cooling thin-film superconducting calorimeters and bolometers that rely on ultra low temperatures. NIS refrigerators cooling from a launch temperature, $T_l=100$ mK could potentially cool to 15 mK. If so, experiments that currently require a dilution refrigerator may be possible with an adiabatic demagnetization or He³ refrigerator, combined with one or more stages of NIS refrigerators. For optimal cooling, the size of the gap Δ in the superconducting electrode of an NIS refrigerator should be roughly ten times $k_b T_l$. An NIS refrigerator cooling from 100 mK based on AlMn with $T_c = 600$ mK has the potential to cool to lower temperature than one based on Al with $T_c = 1300$ mK. The performance of an

NIS refrigerator is dependent upon the sharpness of the gap edge in the BCS density of states. When the NIS refrigerator junctions are biased, a sharp gap edge (low Γ) will cause selective tunneling of electrons such that thermal power is removed from the normal-metal electrode. Increasing Γ smears the gap edge, reducing this selectivity, and degrading the NIS refrigerator performance.

Optimizing Δ improves cooling, while increasing Γ has a negative effect on NIS refrigeration. We used a model for power balance in NIS refrigerators¹² to compare these two effects. Figure 5 shows the calculated base temperature for cooling from $T_l=100$ mK vs Γ with two different Δ values. These results show that an AlMn refrigerator will not perform better than an Al refrigerator because of the increased Γ associated with suppressing Δ .

In order for NIS refrigerators to benefit from optimizing Δ with AlMn, Γ needs to be about a factor of 10 lower than it is in devices made with target T3. If disorder is the dominant source of sub-gap states, it seems unlikely suitable Γ values can be achieved with sputter deposition. However if magnetic effects from the 10 ppm of Fe in T3 are the dominant source of sub-gap states, it is possible that cleaner source material would allow NIS refrigerators to benefit from optimizing Δ with AlMn. While it may be possible to make cleaner AlMn, it is at the least quite difficult based upon our experience acquiring material. If the Γ values result from residual magnetic scattering from Mn, further improvement will not be possible.

There are applications where a shorter quasiparticle lifetime may be desirable. The recovery time constant in Superconducting Kinetic Inductance Detectors (MKID) is set by the quasiparticle lifetime. Shorter lifetimes may enable operation of single photon MKID detectors at higher input count rates¹⁷. Also, AlMn superconducting quasiparticle traps may be more effective with short quasiparticle lifetimes.

VII. CONCLUSIONS

We have made measurements of the DOS and T_c of Aluminum lightly doped with Mn by normal-metal/insulator/superconductor tunneling in very clean AlMn. Kaiser's essential predictions, that the density of states remains BCS-like and the gap reduces in proportion to the transition temperature, are supported. However, additional sub-gap states and gap edge smearing, not predicted by Kaiser, are observed. The origin of these states is not fully understood. Likely possibilities include decreased quasiparticle lifetime due to disorder or to residual magnetic impurities. While shortened quasiparticle lifetimes may be desirable for some applications, gap-smearing and sub-gap states are seldom desirable. In AlMn, these distortions to the BCS DOS outweigh the advantage of a reduced energy gap in NIS refrigerators optimized for cooling below 100 mK.

Acknowledgments

We thank Alan Kaiser for useful discussions and generous donation of computer code. We acknowledge finan-

cial support from the NASA APRA program under grant number NNH09AK271.

-
- [†] Electronic address: oneilg@boulder.nist.gov
- ¹ P. Anderson, *Physical Review* **124**, 41 (1961).
- ² A. A. Abrikosov and L. P. Gor'kov, *JETP* **12**, 1243 (1961).
- ³ A. B. Kaiser, *Journal of Physics C Solid State Physics* **3**, 410 (1970).
- ⁴ G. O'Neil, D. Schmidt, N. A. Miller, J. N. Ullom, A. Williams, G. B. Arnold, and S. T. Ruggiero, *Phys. Rev. Lett.* **1**, 056804 (2008).
- ⁵ D. Akerib, M. Attisha, C. Bailey, L. Baudis, D. Bauer, P. Brink, P. Brusov, R. Bunker, B. Cabrera, D. Caldwell, et al., *Physical Review Letters* **96**, 11302 (2006).
- ⁶ R. D. Horansky, J. N. Ullom, J. A. Beall, G. C. Hilton, K. D. Irwin, D. E. Dry, E. P. Hastings, S. P. Lamont, C. R. Rudy, and M. W. Rabin, *Applied Physics Letters* **93**, 123504 (pages 3) (2008), URL <http://link.aip.org/link/?APL/93/123504/1>.
- ⁷ N. A. Miller, G. C. O'Neil, J. A. Beall, G. C. Hilton, K. D. Irwin, D. R. Schmidt, L. R. Vale, and J. N. Ullom, *Appl. Phys. Lett.* **92**, 163501 (pages 3) (2008), URL <http://link.aip.org/link/?APL/92/163501/1>.
- ⁸ F. Giazotto, T. Heikkilä, A. Luukanen, A. Savin, and J. Pekola, *Reviews of Modern Physics* **78**, 217 (2006).
- ⁹ C. Chen, P. Delsing, D. Haviland, and T. Claeson, *Physica Scripta* **42**, 182 (1992).
- ¹⁰ R. C. Dynes, V. Narayanamurti, and J. P. Garno, *Phys. Rev. Lett.* **41**, 1509 (1978).
- ¹¹ L. Solymar, *Superconducting Tunnelling and Applications* (Wiley - Interscience, 1972).
- ¹² A. M. Clark, A. Williams, S. T. Ruggiero, M. L. van den Berg, and J. N. Ullom, *Appl. Phys. Lett.* **84**, 625 (2004).
- ¹³ R. Barends, S. van Vliet, J. J. A. Baselmans, S. J. C. Yates, J. R. Gao, and T. M. Klapwijk, *Physical Review B (Condensed Matter and Materials Physics)* **79**, 020509 (pages 4) (2009), URL <http://link.aps.org/abstract/PRB/v79/e020509>.
- ¹⁴ H. Shiba, *Progress of theoretical physics* **50**, 50 (1973).
- ¹⁵ J. Zittartz, A. Bringer, and E. Mller-Hartmann, *Solid State Communications* **10**, 513 (1972), ISSN 0038-1098, URL <http://www.sciencedirect.com/science/article/B6TVW-46X9G68-4G/2/8638e8db0715b71e64f8d284355adb34>.
- ¹⁶ A. G. Kozorezov, A. A. Golubov, J. K. Wigmore, D. Martin, P. Verhoeve, R. A. Hijmering, and I. Jerjen, *Physical Review B (Condensed Matter and Materials Physics)* **78**, 174501 (pages 13) (2008), URL <http://link.aps.org/abstract/PRB/v78/e174501>.
- ¹⁷ B. A. Mazin, B. Bumble, P. K. Day, M. E. Eckart, S. Golwala, J. Zmuidzinas, and F. A. Harrison, *Applied Physics Letters* **89**, 222507 (pages 3) (2006), URL <http://link.aip.org/link/?APL/89/222507/1>.